Progress In Electromagnetics Research, Vol. 136, 523–542, 2013

RANGE ALIGNMENT AND MOTION COMPENSATION FOR MISSILE-BORNE FREQUENCY STEPPED CHIRP RADAR

Bo Liu* **and Wenge Chang**

School of Electronic Science and Engineering, National University of Defense Technology, Changsha, Hunan 410073, China

Abstract—One of the difficulties for frequency stepped chirp radar (FSCR) is to resolve the range-Doppler coupling due to relative motion between the radar and the target. Motion compensation is usually adopted to solve the problem in realizing synthetic high range resolution profile (HRRP) for a moving target. For missile-borne FSCR, the range migration of target echo during a coherent processing interval, which is resulted from the high speed motion of missile, is serious and will affect target detection and synthetic high range resolution profile. Therefore, range migration correction and motion compensation are very important for missile-borne FSCR signal processing. In the paper, with the background of terminal guidance anti-ship FSCR seeker, the range alignment is accomplished in frequency domain during the process of real-time digital pulse compression. Then an effective velocity estimation algorithm based on the waveform entropy of the Doppler amplitude spectrum of target echoes is addressed and the velocity estimation accuracy is derived. Finally, the simulation indicates that the new method can estimate the radial velocity accurately and reconstruct the distorted HRRP successfully. In addition, the method has good anti-noise performance and works in the scenario of multi-target with different velocities as well.

1. INTRODUCTION

High range resolution (HRR) radars use wide-band waveforms to resolve individual scatterers within the target [1, 2]. Frequency stepped chirp radar (FSCR) is a kind of HRR radar and is widely used in recent

Received 8 November 2012, Accepted 17 January 2013, Scheduled 23 January 2013
* Corresponding author: Bo Liu (liubo19830120@163.com).

years [3–6], for it can achieve high range resolution while still retaining the advantages of narrow instantaneous receiver bandwidth and low analog-to-digital (AD) sampling rate. FSCR transmits a chirp train with frequency stepped carriers, and achieves high range resolution by synthesis wide-band technique. For HRR radar, the multiple scattering centres of a target may appear in a number of isolated range cells, so the target is called a range-spread target [7, 8]. The high range resolution profile (HRRP) of the target is used for target recognition and high accuracy tracking [9–11], which is very important for missile to improve the tracking ability and attacking accuracy. However, the disadvantage of FSCR is the complication caused by range-Doppler coupling, due to relative motion between the radar and the target, which results in circular shift and the spreading of HRRP [12].

In recent years, some investigations have been proposed to mitigate the distortion of HRRP caused by motion [13–15]. In [13], two successive stepped-frequency pulse trains were transmitted to eliminate the phase errors for the moving target. In [14], a method using multiple stepped-frequency pulse trains and the robust phase unwrapping theorem to estimate the range and the velocity of a target was introduced. However, the methods in [13, 14] need to transmit additional assistant signal, which leads to the amount of available information reduced, and lowers the data rate of the radar. In [15], an algorithm based on the maximum likelihood (ML) estimation is proposed, without altering the conventional stepped-frequency waveform. The algorithm estimates the target velocity accurately; however, the computation consumption is large, so it is difficult to implement in real time. Furthermore, all these methods mentioned above do not consider the range migration of target echo during a coherent processing interval (CPI) [16]. The terminal velocity of missile is so high that the range migration of target echo during a CPI is serious and will affect target detection and synthetic HRRP [17]. Hence, range alignment is necessary for missile-borne FSCR.

In this paper, an effective velocity estimation algorithm based on the waveform entropy (WE) of the Doppler amplitude spectrum of the target echoes is developed for FSCR which is assumed to work in anti-ship seeker. Firstly, the target echo model of missile-borne FSCR is established, and the problem of motion compensation is analyzed. Range alignment is accomplished in frequency domain during the process of digital pulse compression. Secondly, the velocity estimation algorithm based on the WE of the Doppler amplitude spectrum is addressed, and the velocity estimation accuracy is derived. Finally, the simulation indicates that the algorithm can accurately estimate the radial velocity between the radar and the target and reconstruct

the distorted HRRP successfully.

The paper is organized as follows. In Section 2, the signal model of moving targets for FSCR is formulated. In Section 3, we address the velocity estimation method and derive the velocity estimation accuracy. The performance of the proposed method is assessed in Section 4. At last, in Section 5, some conclusions are given.

2. PROBLEM STATEMENT

2.1. Radar Echo Model

The transmitted signal of FSCR is expressed as:

$$s(t) = \sum_{i=0}^{M-1} A_i \cdot u_i(t) e^{j2\pi(f_0+i\Delta f)t} \tag{1}$$

where t is time variable, $u_i(t) = \text{rect}[(t - iT_r)/T_p] \cdot \exp[j\pi\mu(t - iT_r)^2]$ the complex envelop of the i-th chirp sub-pulse, and $\mu = B_c/T_p$ the frequency slope of each chirp sub-pulse,

A_i: amplitude of i-th chirp sub-pulse,

T_r: pulse repetition interval (PRI),

T_p: pulse width of chirp sub-pulse, and $T_p < T_r$,

B_c: band width of each chirp sub-pulse,

f_0: nominal carrier frequency,

Δf: frequency step, $\Delta f < B_c$,

M: number of chirp sub-pulse.

Assuming the radial velocity between the radar and the target remains constant during a CPI, the relative radial velocity is v, and the initial range between the radar and the target is R_0. Demodulated with its corresponding carrier frequency, the target echo is expressed as:

$$\begin{aligned} r(t) &= \sum_{i=0}^{M-1} A_i \cdot u_i\left[t - \tau_i\right] e^{-j2\pi(f_0+i\Delta f+f_{di})\tau_i} \\ &= \sum_{i=0}^{M-1} A_i \cdot \text{rect}\left[\frac{t - iT_r - \tau_i}{T_p}\right] \cdot \exp\left[j\pi\mu(t - iT_r - \tau_i \underbrace{-f_{di}/\mu}_{range\_Doppler\_coupling})^2\right] \\ &\quad \cdot e^{-j2\pi(f_0+i\Delta f+f_{di})\tau_i} \end{aligned} \tag{2}$$

where $\tau_i = 2(R_0 - ivT_r)/c$, c is the speed of light, τ_i the delay of the i-th chirp sub-pulse, and $f_{di} = 2v(f_0 + i\Delta f)/c$ the Doppler frequency

of the i-th chirp sub-pulse echo. From Equation (2), it can be seen that the relative radial velocity between the radar and the target produces range-Doppler coupling to chirp signal [18], which results in mismatching between the target echo and the matched filter.

After matched filtering, a group of compressed pulses can be obtained:

$$y(i,t) = \sum_{i=0}^{M-1} A_i \sqrt{\mu T_p^2} \cdot \mathrm{rect}\left[\frac{t-iT_r-\tau_i}{T_p}\right] \cdot \frac{\sin\left[\pi B_c(t-iT_r-\tau_i-f_{di}/\mu)\right]}{\pi B_c(t-iT_r-\tau_i-f_{di}/\mu)} \cdot \left(1-\frac{|t-iT_r-\tau_i|}{T_p}\right) \cdot e^{j\pi/4} \cdot e^{-j2\pi\left[(f_0+i\Delta f+f_{di})\tau_i+\frac{1}{2}\mu(t-iT_r-\tau_i)^2\right]}, \quad i=0,1,2,\ldots,M-1. \tag{3}$$

Due to mismatching, envelops of the pulse compression results in Equation (3) are not Sinc functions any more. According to [18], the amplitude loss in Equation (3) is negligible, but the time shift resulting from the time-frequency coupling of chirp signal is significant and will affect the range measurement accuracy. Additionally, for missile-borne radar, the radial velocity v between the radar and the target produces serious range migration during a CPI. From Equation (3), the migration time between the adjacent pulses can be written as:

$$\Delta t = 2v(T_r - \Delta f/u)/c \tag{4}$$

Range migration factor P is defined as:

$$P = B_c(M-1)\Delta t = B_c 2v(M-1)(T_r - \Delta f/\mu)/c \tag{5}$$

The range migration factor P represents the number of the range resolution cell that the target echo spreads in the coarse resolution domain during a CPI.

Sampling at $t = iT_r - \tau_i$, the phases of the M samples from the compressed pulses in Equation (3) are expressed as:

$$\begin{aligned}\phi_i = &\frac{\pi}{4} - \frac{4\pi f_0 R_0}{c} + \frac{4\pi f_0 v T_r}{c} i - \frac{4\pi \Delta f R_0}{c} i + \frac{4\pi \Delta f v T_r}{c} i^2 \\ &- \frac{8\pi f_0 R_0 v}{c^2} - \frac{8\pi R_0 v \Delta f}{c^2} i + \frac{8\pi v^2 f_0 T_r}{c^2} i + \frac{8\pi v^2 T_r \Delta f}{c^2} i^2 \\ \approx &\underbrace{\left(\frac{\pi}{4} - \frac{4\pi f_0 R_0}{c} - \frac{4\pi \Delta f R_0}{c} i\right)}_{inherent\_phase\_terms} - \underbrace{\left(\frac{8\pi f_0 R_0 v}{c^2} - \frac{4\pi f_0 v T_r}{c} i - \frac{4\pi \Delta f v T_r}{c} i^2\right)}_{additional\_phase\_terms}, \quad i=0,1,2,\ldots,M-1. \end{aligned} \tag{6}$$

The expansion of the phase component ϕ_i can be seen as two parts: the inherent phase terms and the additional phase terms resulting from radial motion.

If $v = 0$, the synthetic HRRP of the target can be obtained by taking the M-point inverse discrete Fourier transform (IDFT) of the collected M samples [19], which is given by:

$$|z(l)| = \left| \frac{\sin\left[\pi M \Delta f \left(\frac{l}{M\Delta f} - \frac{2R_0}{c}\right)\right]}{M \sin\left[\pi \Delta f \left(\frac{l}{M\Delta f} - \frac{2R_0}{c}\right)\right]} \right|, \quad l = 0, 1, \ldots, M-1. \tag{7}$$

However, if $v \neq 0$, the additional motion phase terms in Equation (6) will result in target distortion in the synthetic HRRP [12]. Precisely, the linear component of the additional phase term $4\pi f_0 v T_r i/c$ causes the circular range shifting, while the quadratic component $4\pi \Delta f v T_r i^2/c$ produces spreading for HRRP [20]. Both of them are significant distortions for HRRP. Particularly, for missile-borne FSCR, the target spreading is considerably more significant than the target shifting because target spreading degrades the desired range resolution and decreases the signal-to-noise ratio (SNR), which will influence target recognition and high accuracy tracking. Nevertheless, once the radial velocity is able to be estimated, the additional motion phase term can be compensated and the HRRP can be reconstructed [20]. The velocity compensation accuracy for the quadratic phase is given by [20]:

$$|\Delta v| < c/\left[8(M-1)^2 \Delta f T_r\right] \tag{8}$$

And the velocity compensation accuracy for the linear phase is given by:

$$|\Delta v| < c/(4M f_0 T_r) \tag{9}$$

Additionally, if $v \neq 0$, the range migration of echo data during a CPI in Equation (4) will affect the following signal processing of FSCR. Firstly, the range migration degrades the range measurement accuracy. Secondly, the range migration during a CPI disperses the energy of the target echo, which makes it more difficult to detect target. And finally, it affects the synthetic HRRP of the target [20].

The parameters of a FSCR are listed in Table 1, which are assumed according to the principle in [1]. Henceforth, without loss of generality, the simulation and illustration both adopt the parameters in Table 1.

The range migration factors resulting from radial velocity between the radar and the target are listed in Table 2. Figure 1 shows the

Table 1. Parameters of a FSCR.

f_0	B_c	Δf	M	T_p	T_r
35 GHz	10 MHz	2 MHz	128	20 μs	200 μs

Table 2. Range migration factors resulting from radial velocity between the radar and the target.

missile velocity (m/s)	1000	1500	2000	2500	3000	4000
P (coarse range resolution cell)	1.67	2.49	3.32	4.15	4.98	6.64

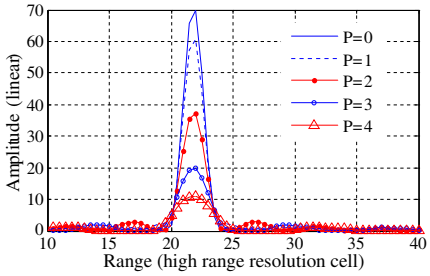

Figure 1. HRRPs at different range migration factor P.

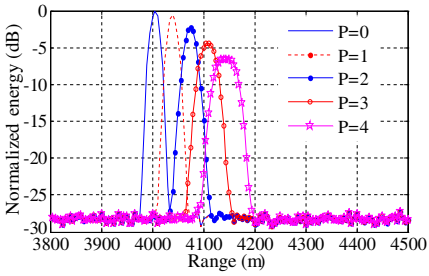

Figure 2. Incoherent integration results at different range migration factor P.

HRRPs of a point-like target with different range migration factors, amusing that the additional motion phase terms in Equation (6) has been compensated thoroughly. As can be seen from Figure 1, the range migration decreases the amplitude of the HRRP, the more the range migration, the more the amplitude loss will be. While the range migration factor $P = 2$, the amplitude of HRRP is about a half of that of the ideal HRRP. In other words, the amplitude loss is about -3 dB when the range migration factor $P = 2$. The incoherent integration results of radar echo with different range migration are shown in Figure 2, from which we can see that the range migration spreads the energy of target echo, which is harmful to target detection. In addition, the position of the target moves, which degrades the range measurement accuracy of FSCR.

Assume that it is required that the range migration during a CPI is no more 1/4 coarse range resolution cell [20]. According to Equation (5), the radial velocity between the radar and the target should satisfy the following equation:

$$v < \frac{c}{8B_c(T_r - \Delta f/\mu)(M-1)} \tag{10}$$

2.2. Range Alignment

For missile-borne radar, Equation (10) usually cannot be satisfied. Therefore, it is necessary to correct the range migration between the HRRPs before target detection and synthesizing HRRP. Assume that the velocity of missile v_m can be obtained by the missile-borne inertial navigation system (INS) [21]. Setting the velocity measurement error by the INS is Δv_m. If we adopt v_m as a coarse estimation of the radial velocity between the radar and the target, the estimation error can be written as:

$$\varepsilon = \Delta v_m + v_t \tag{11}$$

where v_t is the radial velocity of the target ship.

For missile-borne FSCR, the coarse estimation of the radial velocity above is not accurate enough to be up to the accuracy of motion phase compensation [22]. However, for range migration correction, the coarse estimation of the radial velocity is adequate. Therefore, we adopt the coarse estimation of the radial velocity v_m to align the range migration during a CPI.

Utilizing the time-frequency symmetry properties of Fourier transform, range alignment can be accomplished in frequency domain. Firstly, transform the pulse compression results in Equation (3) to frequency domain by the fast Fourier transform (FFT). Then multiply them by the corresponding frequency domain phase terms with respect to the radial velocity. Finally, transform the products to time domain again by the inverse fast Fourier transform (IFFT) and the range alignment result can be obtained:

$$\begin{aligned} y'(i,t) &= \mathrm{IFFT}\left\{ y(i,f) \cdot e^{j4\pi v_m[(f_0+i\Delta f)/\mu - iT_r]f/c} \right\} \\ &\approx A_i \sqrt{\mu T_p^2} \cdot \mathrm{rect}\left[\frac{t - iT_r - 2R_0/c}{T_G} \right] \cdot \mathrm{sinc}\left[\pi B_c \left(t - iT_r - \frac{2R_0}{c} \right) \right] \\ &\quad \cdot e^{j\pi/4} \cdot e^{-j2\pi\left[(f_0+i\Delta f+f_{di})\tau_i + \frac{1}{2}\mu(t-iT_r-2R_0/c)^2\right]} + C'(t), \\ &\qquad i = 0, 1, 2, \ldots, M-1. \end{aligned} \tag{12}$$

where $y'(i,\, t)$ is the compressed pulses after range alignment, $y(i, f) = \mathrm{FFT}[y(i,\, t)]$. Although the process of the range alignment above needs abundant computation, it does not take much additional time in the signal processing, because it could be accomplished concurrently with digital pulse compression. Figure 3 illustrates the approach of range alignment during the pulse compression with digital matched filter.

Supposing that the velocity of missile v_m provided by the INS is 2000 m/s, the real radial velocity between the missile and the target $v = 2025$ m/s, and the error of the coarse estimation of the radial velocity $\varepsilon = 25$ m/s. The initial range of a point-like target is 4000 m.

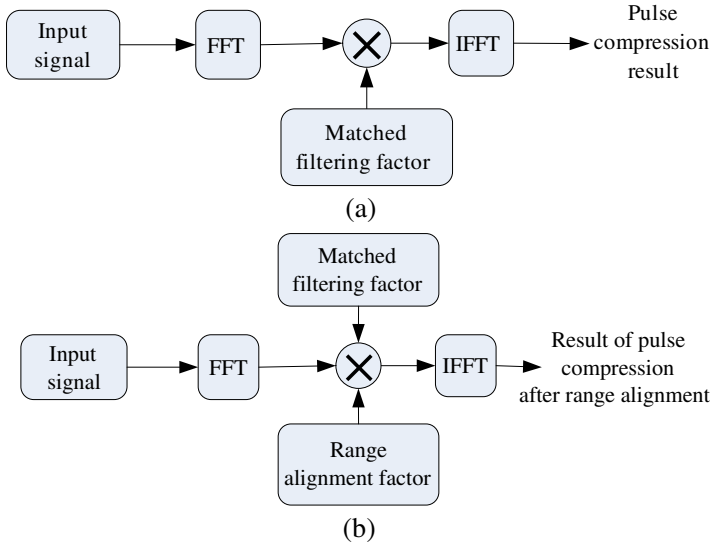

Figure 3. Range alignment during the digital pulse compression. (a) Conventional digital pulse compression with matched filter. (b) Range alignment during the digital pulse compression.

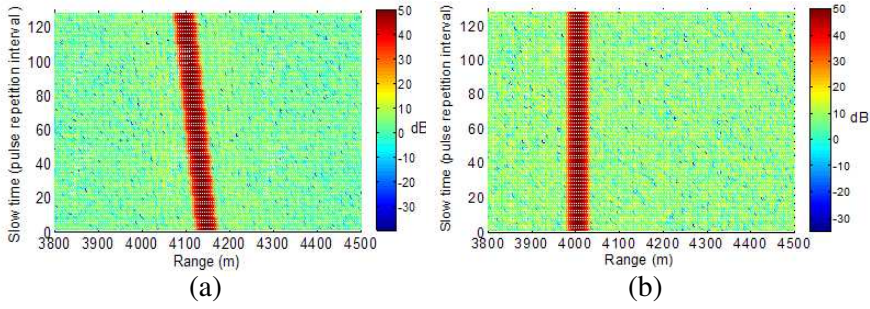

Figure 4. Top view of target echoes after pulse compression. (a) Without range alignment. (b) After range alignment.

According to Equation (5) and the radar parameters in Table 1, the range migration factor P is 3.36 before range alignment and 0.04 after range alignment with the coarse estimation of the radial velocity v_m. The top view of target echoes are shown in Figure 4, where Figure 4(a) is the target echoes without range alignment and Figure 4(b) the target echoes after range alignment. Figure 5 shows the benefits of range

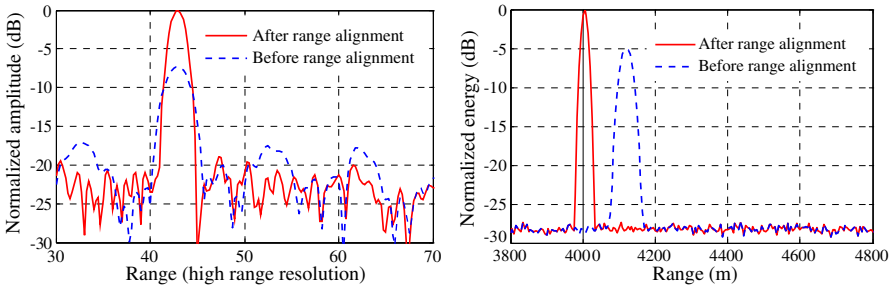

Figure 5. The benefits of range alignment to HRRP and incoherent integration. (a) HRRPs before and after range alignment. (b) Incoherent integration results before and after range alignment, initial range of the target $R_0 = 4000\,\mathrm{m}$.

alignment to HRRP and incoherent integration, where Figure 5(a) compares the HRRP before and after range alignment, as can be seen that the amplitude of HRRP increases about 7 dB after range alignment. Figure 5(b) illustrates the incoherent integration results before and after range alignment. We can see that the signal-to-clutter ratio (SCR) has about 5 dB improvement after range alignment. Moreover, the range error caused by the range migration and time-frequency coupling of chirp signal has been corrected effectively.

3. VELOCITY ESTIMATION AND MOTION COMPENSATION

3.1. Radial Velocity Estimation

The velocity estimation method based on the Doppler shift has high accuracy [23]. However, missile-borne FSCR usually works with a low pulse repetition frequency (LPRF) waveform which is unambiguous in range but mostly ambiguous in Doppler. According to the radar theory [24], the most unambiguous Doppler velocity of FSCR is:

$$v_{\max} = c \cdot f_{prf} / (2 f_0) \tag{13}$$

where f_{prf} is the pulse repetition frequency (PRF), $f_{prf} = 1/T_r$. The velocity resolution cell is:

$$v_{cell} = v_{\max}/M = c \cdot f_{prf} / (2M f_0) \tag{14}$$

Let's have a closer look at the phase component ϕ_i in Equation (6).

Setting $f_{d0} = 2vf_0/c$, Equation (6) can be rewritten as:

$$\phi_i = \underbrace{\left(\frac{\pi}{4} - \frac{4\pi f_0 R_0}{c} - \frac{8\pi f_0 R_0 v}{c^2} + 2\pi f_{d0} T_r i\right)}_{phase\_terms\_of\_pulsed\_Doppler\_radar} - \underbrace{\left(\frac{4\pi \Delta f R_0}{c} i - \frac{4\pi \Delta f v T_r}{c} i^2\right)}_{additional\_phase\_terms\_by\_\Delta f},$$
$$i = 0, 1, 2, \ldots, M-1. \quad (15)$$

The phase component ϕ_i can be seen as another two parts: the phase terms of a pulsed Doppler radar with carrier-frequency f_0 and the additional phase terms. For pulsed Doppler radars, coherent processing is implemented by the discrete Fourier transform (DFT) as a matched filter [24]. Processing the sampled echo data of the same carrier-frequency via DFT, the Doppler amplitude spectrum will yields at the Doppler frequency point. From Equation (11), we can see that the frequency step Δf and the initial range R_0 introduce an additional phase $(4\pi\Delta f R_0/c)i$, which will result in a circular shift of the Doppler frequency within the unambiguous DFT window after coherent processing, which is called the range-Doppler coupling effect [25]. The final term is a quadratic phase $4\pi\Delta f v T_r i^2/c$, whose effects are shown in widening and distortion of the main lobe of the Doppler amplitude spectrum. In other words, this term results in energy dispersion of the Doppler amplitude spectrum along the Doppler axis.

Consequently, if the initial range R_0 is known, the range-Doppler coupling term $(4\pi\Delta f R_0/c)i$ can be removed by phase compensation. We call it resolving the range-Doppler coupling. In addition, the Doppler ambiguity can be resolved by using the effects of the quadratic phase term $(4\pi\Delta f v T_r/c)i^2$ on the Doppler amplitude spectrum. The initial range of the target R_0 has been obtained by target detection in the coarse resolution domain. After resolving the range-Doppler coupling and motion pre-compensation with the coarse velocity estimation v_m to Equation (6), the phase component of target echo can be rewritten as:

$$\phi_i' = \frac{\pi}{4} - \frac{4\pi f_0 R_0}{c} - \frac{8\pi f_0 R_0 v}{c^2} + 2\pi f_{d0} T_r i - \frac{4\pi \Delta f \Delta R}{c} i + \frac{4\pi \Delta f \Delta v T_r}{c} i^2,$$
$$i = 0, 1, 2, \ldots, M-1. \quad (16)$$

where ΔR is the range error and Δv the velocity error.

According to the radar parameters in Table 1, the most unambiguous velocity $v_{\max} = 21.4286\,\mathrm{m/s}$. Setting the radial velocity between the radar and the target is 2000 m/s, the Doppler frequency $f_{d0} = 4.6667 \times 10^5\,\mathrm{Hz}$. Figure 6 shows the effects of the residual quadratic phase term $(4\pi\Delta f \Delta v T_r/c)i^2$ on the Doppler amplitude spectrum.

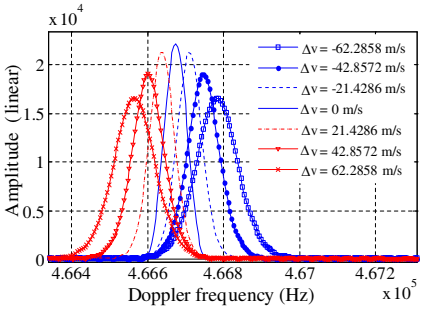

Figure 6. Quadratic phase effects on Doppler amplitude spectrum.

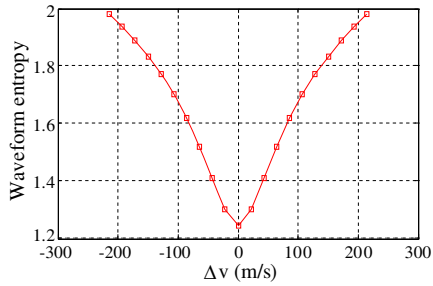

Figure 7. The variation curve of the Doppler amplitude spectrum's WE with the pre-compensation velocity error.

Entropy is a measure of the uncertainty of random variables [26]. In [27–30], the waveform entropy (WE) is introduced and adopted to survey the dispersion degree of a waveform's energy with respect to its parametric axis. Supposing the sampled signal waveform is denoted as $A(n)$, $n = 1, 2, \ldots, N$, setting:

$$\begin{cases} p(n) = |A(n)| / \|A\| \\ \|A\| = \sum_{n=1}^{N} |A(n)| \end{cases}, \quad n = 1, 2, \ldots, N. \tag{17}$$

Then the WE of $A(n)$ is defined by:

$$WE\left[A(n)\right] = -\sum_{n=1}^{N} p(n) \cdot \log_2 p(n) \tag{18}$$

According to the definition above, the waveform entropy has the following properties:

(1) $E[A(n)] \to 0$, when $p(n) \to 0$, the sparser $A(n)$ is, the smaller $WE[A(n)]$ will be.

(2) $E[A(n)] \leq \log_2 N$, the equation comes into existence when $p(n) = 1/N$, $\forall n = 0, 1, \ldots, N-1$, the more homogeneous the distribution of $A(n)$'s energy is, the larger $WE[A(n)]$ will be.

If the energy of $A(n)$ distributes uniformly along its parametric axis, the WE reaches the maximum. On the contrary, if the energy concentrates only on one sampling point, the WE is the minimum. Accordingly, the WE, served as a measure function, can be employed to

weigh the effects of the quadratic phase term on the Doppler amplitude spectrum. The WE of the Doppler amplitude spectrum with different pre-compensation velocity error Δv are shown in Figure 7. As we can see, while the velocity error $\Delta v = 0$, the WE of the Doppler amplitude spectrum is the minimum.

As a result, a velocity estimation based on the WE of the Doppler amplitude spectrum can be realized in the following three steps:

Firstly, resolve the range-Doppler coupling of FSCR by the initial range of the target R_0 estimated by target detection.

Secondly, make a preliminary estimate of the radial velocity. The maximum of the coarse velocity measurement error ε is usually known. In the velocity interval $[v_m - \varepsilon_{\max}, v_m + \varepsilon_{\max}]$, where $\varepsilon_{\max}$ is the maximum of ε, with a step of $v_{\max}$, the preliminary velocity estimate $\hat{v}_1$ can be achieved by searching for the position on the Δv axis, where the minimum value of the WE is located.

And finally, make an accurate estimation of radial velocity. The radial velocity between the radar and the target can be expressed as:

$$v = k \cdot v_{\max} + n_0 \cdot v_{cell} \tag{19}$$

where k is the Doppler ambiguity number and n_0 the index of the Doppler axis, which can be obtained by coherent processing [24]. It is easy to find k_0 which satisfies the following equation:

$$(k_0 \cdot v_{\max} + n_0 \cdot v_{cell}) \le \hat{v}_1 < [(k_0 + 1) \cdot v_{\max} + n_0 \cdot v_{cell}] \tag{20}$$

Using $k_0 \cdot v_{\max} + n_0 \cdot v_{cell}$ and $(k_0+1) \cdot v_{\max} + n_0 \cdot v_{cell}$ to compensate the motion quadratic phase, respectively, whichever makes the EW of the Doppler amplitude spectrum smaller is chosen as the final estimation of the radial velocity. In other words, the accurate estimation of the radial velocity $\hat{v}$ can be given as:

$$\hat{v} = \arg \cdot \min \left\{ WE \left[(k \cdot v_{\max} + n_0 \cdot v_{cell}) - v \right], k = k_0, k_0 + 1 \right\} \tag{21}$$

where $WE[\cdot]$ is the WE of the Doppler amplitude spectrum, which is a function of the velocity estimation error.

3.2. The Velocity Estimation Accuracy and Targets Imaging

After compensation to the quadratic phase by the preliminary velocity estimate $\hat{v}_1$, the effect of the motion quadratic phase on the Doppler amplitude spectrum can be negligible. As a result, the velocity estimation error mainly depends upon the range-Doppler coupling shift resulting from the range measure error ΔR. Equation (16) can be rewritten as:

$$\varphi_i' = \frac{\pi}{4} - \frac{4\pi f_0 R_0}{c} - \frac{8\pi f_0 R_0 v}{c^2} + 2\pi \left(f_{d0} - \frac{2\Delta f \Delta R}{c} f_{prf} \right) T_r i + \frac{4\pi \Delta f \Delta v T_r}{c} i^2, \quad i = 0, 1, 2, \ldots, M-1. \tag{22}$$

After range migration correction by v_m, the coarse velocity error ε can also produce slight range migration between adjacent pulses and time-frequency coupling to chirp pulses. According to Equation (5), the range migration induced by the coarse velocity measurement error ε is written as:

$$\Delta P = 2B_c\varepsilon(M-1)(T_r - \Delta f/\mu)/c \tag{23}$$

The range measurement error caused by ΔP can be written as:

$$\Delta r_1 = -\Delta P \cdot c/(2B_c) = -\varepsilon(M-1)(T_r - \Delta f/\mu) \tag{24}$$

The range measurement error caused by time-frequency coupling of the chirp sub-pulse is:

$$\Delta r_2 = \varepsilon \cdot f_0/\mu \tag{25}$$

Therefore, the total range measurement error is:

$$\Delta R = |\Delta r_1 + \Delta r_2| \tag{26}$$

By substituting ΔR into Equation (22), the velocity estimation error of the proposed method can be obtained:

$$e = \frac{|f_0/\mu - (M-1)(T_r - \Delta f/\mu)|\Delta f\varepsilon}{f_0 T_r} < \frac{\Delta f}{B_c} \cdot \frac{T_p}{T_r} \cdot \varepsilon \tag{27}$$

Substituting the radar parameters of Table 1 into the above equation, the radial velocity estimation error can be obtained:

$$e = 0.0129\varepsilon \tag{28}$$

After compensation to the additional phase in Equation (6) by the velocity estimation $\hat{v}$, the synthetic HRRP of the target can be obtained by the IDFT [22]. It should be pointed out that the initial range information of the targets has been obtained by target detection before velocity estimation, therefore, the velocity estimation and motion compensation can be carried out just to the target echo data instead of the data of whole frame [14]. Consequently, the proposed method can work in the scenario of multiple-target with different velocities. Figure 8 is the flow chart of the proposed motion compensation and target imaging method.

4. PERFORMANCE ASSESSMENT

In order to investigate the effectiveness of the proposed method, a simulation is carried out based on the radar parameters in Table 1. The sea clutter is assumed to be much greater than the receiver thermal noise, thus thermal noise can be ignored [31, 32]. Meanwhile, the clutter is assumed to be Gaussian distributed with zero-mean, and

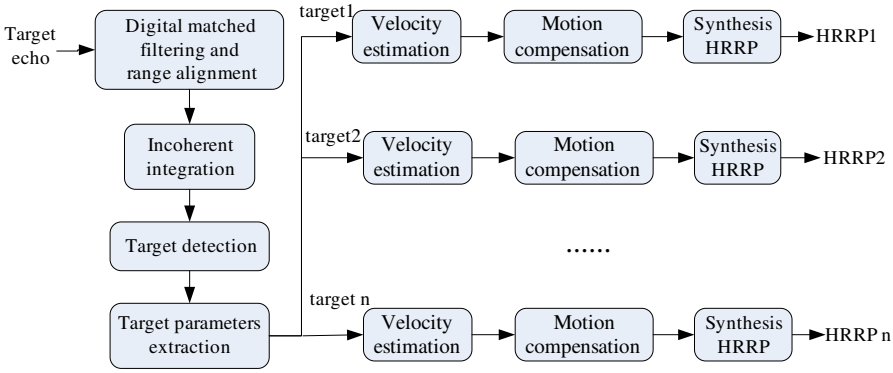

Figure 8. Flow chart of the proposed algorithm.

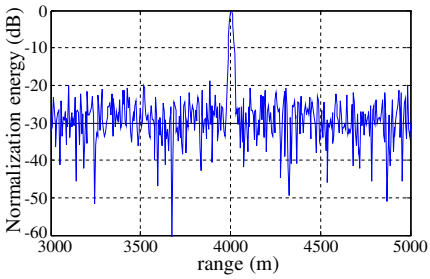

Figure 9. Pulse compression result of the target echo (SCR = 30 dB).

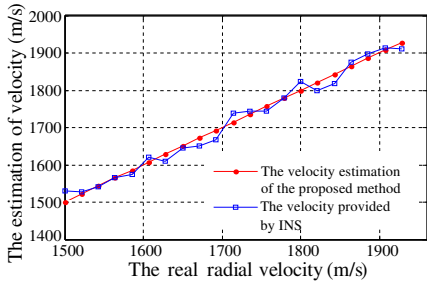

Figure 10. Radial velocity estimation results (SCR = 30 dB, $\varepsilon = 30$ m/s).

independent from range cell to range cell. Setting the SCR of the target echo (after pulse compression) is 30 dB, as shown in Figure 9. Figure 10 compares the velocity estimation result of the proposed method and the coarse velocity provided by missile-borne INS, where the coarse velocity error $\varepsilon = 30$ m/s. The estimation error is shown in Figure 11, it can be seen that the estimation error of the proposed method is much smaller than the coarse estimation error ε. Equation (27) indicates that the estimation error of the proposed method e is proportional to the coarse velocity error ε, Figure 12 shows the velocity estimation errors with different coarse velocity errors.

From Figures 10–12, we can see that the proposed algorithm can estimate the radial velocity between the radar and the target effectively, which is accurate enough to be up to the quadratic motion phase compensation for FSCR [22].

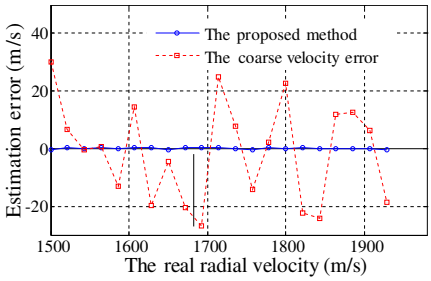

Figure 11. Velocity estimation error (SCR = 30 dB, ε = 30 m/s).

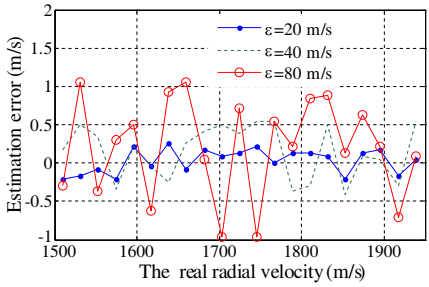

Figure 12. Velocity estimation errors with different coarse velocity errors (SCR = 30 dB).

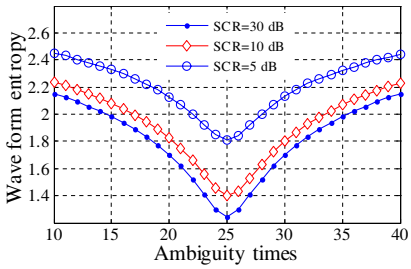

Figure 13. Resolving Doppler ambiguity under different SCRs.

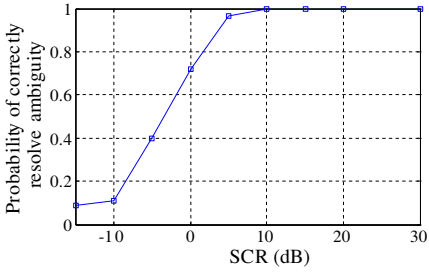

Figure 14. Curve of the anti-noise performance.

Resolving Doppler ambiguity is the key of the proposed algorithm. Assuming the radial velocity v = 550 m/s, according to the radar parameters in Table 1, the most unambiguous velocity $v_{\max}$ = 21.4286 m/s. Therefore, the radial velocity can be written as:

$$v = 25 \cdot v_{\max} + 14.285 \text{ m/s} \tag{29}$$

Therefore, the ambiguity number k = 25. The result of resolving Doppler ambiguity results under different SCR are shown in Figure 13. It can be seen that the waveform entropy of the Doppler amplitude spectrum runs to the minimum while the ambiguity number is 25. Figure 14 gives the anti-noise performance of the proposed method. The horizontal is the SCR of the target echo, and the ordinate is the probability of correctly resolving ambiguity. From Figure 14, the proposed method will achieve a reliable ambiguity resolving as long as the SCR is more than 10 dB. Hence, the anti-noise performance of the proposed algorithm is fine.

Finally, the velocity compensation result of a moving target is simulated by computer. Suppose that the range migration of target

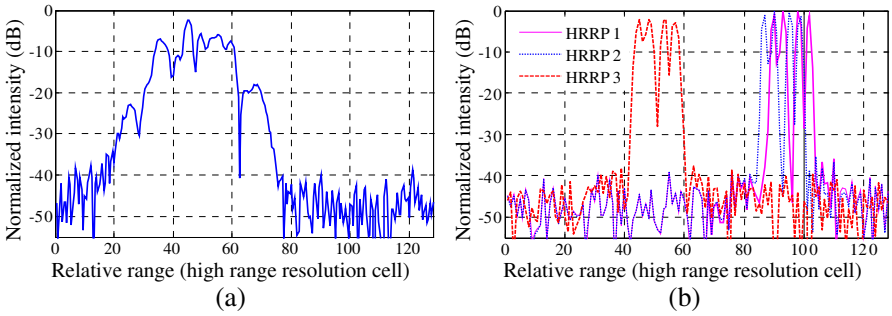

Figure 15. Synthetic HRRP. (a) HRRP without motion compensation. (b) HRRPs after motion compensation. (HRRP1: the ideal HRRP; HRRP2: compensated by the velocity estimation with the proposed method; HRRP3: compensated by the coarse velocity provided by the INS.).

echo has been corrected with the coarse velocity estimation v_m by the range alignment method proposed in Section 2. The target has four scattering centers with the same radial velocity, and the real radial velocity between the radar and the target is 550 m/s. The HRRP of the target, as shown in Figure 15(a), dispersed seriously without velocity compensation. The coarse velocity v_m provided by the missile-borne INS is 520 m/s, the accurate radial velocity estimation $\hat{v}$ obtained by the proposed algorithm is 550.35 m/s. Figure 15(b) shows the ideal HRRP of the target and the HRRPs compensated by $\hat{v}$ and v_m, respectively. Where HRRP1 is ideal, HRRP2 is the result compensated by $\hat{v}$, and HRRP3 is the result compensated by v_m.

It can be seen that compared to HRRP1, HRRP3 has resolution and amplitude loss, and HRRP2 has higher amplitude and range resolution than HRRP3 and almost no distortion. The difference between HRRP2 and HRRP1 is that HRRP2 has a shift of about two high resolution cells.

5. CONCLUSION

The disadvantage of FSCR is the complication caused by range-Doppler coupling, due to relative motion between the radar and the target, which results in circular shift and the spreading of HRRP. Motion compensation is generally adopted to solve the problem in realizing synthetic HRRP for a moving target. An effective velocity estimation algorithm based on the waveform entropy (WE) of the Doppler amplitude spectrum of the target echoes is developed for

FSCR which is assumed to work in anti-ship radar seeker. The target echo model of missile-borne FSCR is established, and the range alignment is accomplished in frequency domain firstly. Then, the velocity estimation algorithm based on the WE of the Doppler amplitude spectrum is addressed, and the velocity estimation accuracy is derived. The simulation indicates that the algorithm can accurately estimate the radial velocity between the radar and the target and reconstruct the distorted HRRP successfully. In fact, Doppler frequency estimation for FSCR is the main idea behind the proposed algorithm, which is accomplished by resolving the range-Doppler coupling and the Doppler ambiguity.

It should be pointed out that the proposed method also works in the scenario of multi-target with different velocities and has good anti-noise performance. Moreover, the method needs not to transmit and receive assistant waveform, and the computational consumption is acceptable for missile-borne radar signal processing. However, the coarse velocity estimation (provided by the missile-borne INS) is needed in the proposed method, and the sea clutter is assumed to be Gaussian distributed, which is an insufficiency for the paper. Further study on more adaptive velocity estimation algorithm in non-Gaussian sea clutter [33, 34] for FSCR will be discussed in our next study.

ACKNOWLEDGMENT

The authors wish to thank the editors, reviewer 1, reviewer 2, reviewer 3, and reviewer 4, whose comments and suggestions helped to improve the contents of the paper.

REFERENCES

1. Wehner, D. R., *High-resolution Radar*, Chapter 4–Chapter 5, Artech House, Boston, 1995.
2. Xu, H.-Y., H. Zhang, K. Lu, and X.-F. Zeng, "A holly-leaf-shaped monopole antenna with low RCS for UWB application," *Progress In Electromagnetics Research*, Vol. 117, 35–50, 2011.
3. Park, S.-H., H.-T. Kim, and K.-T. Kim, "Stepped-frequency ISAR motion compensation using particle swarm optimization with an island model," *Progress In Electromagnetics Research*, Vol. 85, 25–37, 2008.
4. Chua, M. Y. and V. C. Koo, "FPGA-based chirp generator for high resolution UAV SAR," *Progress In Electromagnetics Research*, Vol. 99, 71–88, 2009.

5. Crowgey, B. R., E. J. Rothwell, L. C. Kempel, and E. L. Mokole, "Comparison of UWB short-pulse and stepped-frequency radar systems for imaging through barriers," *Progress In Electromagnetics Research*, Vol. 110, 403–419, 2010.
6. Zhai, W. and Y. Zhang, "Application of super-SVA to stepped chirp radar imaging with frequency band gaps between subchirps," *Progress In Electromagnetics Research B*, Vol. 30, 71–82, 2011.
7. Liu, B. and W. Chang, "A novel range-spread target detection approach for frequency stepped chirp radar," *Progress In Electromagnetics Research*, Vol. 131, 275–292, 2012.
8. Hao, C., F. Bandiera, J. Yang, D. Orlando, S. Yan, and C. Hou, "Adaptive detection of multiple point-like targets under conic constraints," *Progress In Electromagnetics Research*, Vol. 129, 231–250, 2012.
9. Han, S.-K., H.-T. Kim, S.-H. Park, and K.-T. Kim, "Efficient radar target recognition using a combination of range profile and time-frequency analysis," *Progress In Electromagnetics Research*, Vol. 108, 131–140, 2010.
10. Fu, J.-S. and W.-L. Yang, "KFD-based multiclass synthetical discriminant analysis for radar HRRP recognition," *Journal of Electromagnetic Waves and Applications*, Vol. 26, Nos. 2–3, 169–178, 2012.
11. Zhou, D., X. Shen, and Y. Liu, "Nonlinear subprofile space for radar HRRP recognition," *Progress In Electromagnetics Research Letters*, Vol. 33, 91–100, 2012.
12. Zhu, F., Q. Zhang, Q. Lei, and Y. Luo, "Reconstruction of moving target's HRRP using sparse frequency-stepped chirp signal," *IEEE Sensors Journal*, Vol. 11, No. 10, 2327–2334, 2011.
13. Chen, H.-Y., Y.-X. Liu, W.-D. Jiang, and G.-R. Guo, "A new approach for synthesizing the range profile of moving targets via stepped-frequency waveforms," *IEEE Geoscience and Remote Sensing Letters*, Vol. 3, No. 3, 406–409, 2006.
14. Li, G., H. D. Meng, X. G. Xia, and Y. N. Peng, "Range and velocity estimation of moving targets using multiple stepped-frequency pulse trains," *Sensors*, No. 8, 1343–1350, 2008.
15. Liu, Y. M., H. D. Meng, H. Zhang, and X. Q. Wang, "Motion compensation of moving targets for high range resolution stepped-frequency radar," *Sensors*, No. 8, 3429–3437, 2008.
16. Park, S.-H., J.-I. Park, and K.-T. Kim, "Motion compensation for squint mode spotlight SAR imaging using efficient 2D interpolation," *Progress In Electromagnetics Research*, Vol. 128,

503–518, 2012.

17. Kirkland, D. M., "An alternative range migration correction algorithm for focusing moving targets," *Progress In Electromagnetics Research*, Vol. 131, 227–241, 2012.
18. Tao, R., N. Zhang, and Y. Wang, "Analysing and compensating the effects of range and Doppler frequency migrations in linear frequency modulation pulse compression radar" *IET Radar Sonar and Navigation*, Vol. 5, No. 1, 12–22, 2011.
19. Levanon, N., "Stepped-frequency pulse-train radar signal," *IEE Proceedings Radar, Sonar and Navigation*, Vol. 149, No. 6, 297–309, 2002.
20. Sun, H. X., Z. Liu, and Y. H. Cao, "Estimation of a high-velocity target's motion parameters for a modulated frequency stepped radar," *Journal of Xidian University*, Vol. 38, No. 1, 136–141, 2011.
21. Moore, T. A., et al., "Use of the GPS aided inertial navigation system in the navy standard missile for the BMDO/Navy LEAP technology demonstration program," *Proceedings of ION GPS-95*, Palm Springs, CA, September 12–15, 1995.
22. Ma, Y.-B., "Velocity compensation in stepped frequency radar," Master's Thesis, Naval Postgraduate School, California, USA, 1995.
23. Calvo-Gallego, J. and F. Pérez-Martínez, "Simple traffic surveillance system based on range-Doppler radar images," *Progress In Electromagnetics Research*, Vol. 125, 343–364, 2012.
24. Stimson, G. W., *Introduction to Airborne Radar*, 2nd edition, Ch. 15, SciTech Publishing, Inc., Raleigh, 1998.
25. Tian, B., D.-Y. Zhu, and Z.-D. Zhu, "A novel moving target detection approach for dual-channel SAR system," *Progress In Electromagnetics Research*, Vol. 115, 191–206, 2011.
26. Martyushev, L. M. and V. D. Seleznev, "Maximum entropy production principle in physics, chemistry and biology," *Physics Reports*, Vol. 426, 1–10, 2006.
27. Xi, L., "Auto focusing of ISAR images based on entropy minimization," *IEEE Trans. on Aerospace Electron. Syst.*, Vol. 35, No. 4, 1240–1252, 1999.
28. Jing, L., L. X. Guo, and W. Wu, "Application of waveform entropy method for motion compensation to MMW costas frequency hopped radar," *Journal of Infrared and Millimeter Wave*, Vol. 22, No. 4, 303–306, 2003.
29. Xu, S., P. Shui, and X. Yan, "CFAR detection of range-

spread target in white Gaussian noise using waveform entropy," *Electronics Letters*, Vol. 46, No. 9, 647–649, 2010.

30. Zhang, Z.-B., X.-Y. Du, and W.-D. Hu, "Waveform entropy-based target detection in HRRPs," *Aeronautical Computing Technique*, Vol. 37, No. 6, 51–54, 2007.
31. Zhang, J.-P., Z.-S. Wu, Y.-S. Zhang, and B. Wang, "Evaporation duct retrieval using changes in radar sea clutter power versus receiving height," *Progress In Electromagnetics Research*, Vol. 126, 555–571, 2012.
32. Wu, Z.-S., J.-P. Zhang, L.-X. Guo, and P. Zhou, "An improved two-scale model with volume scattering for the dynamic ocean surface," *Progress In Electromagnetics Research*, Vol. 89, 39–56, 2009.
33. Luo, W., M. Zhang, C. Wang, and H.-C. Yin, "Investigation of low-grazing-angle microwave backscattering from three-dimensional breaking sea waves," *Progress In Electromagnetics Research*, Vol. 119, 279–298, 2011.
34. Qi, C., Z. Zhao, W. Yang, Z.-P. Nie, and G. Chen, "Electromagnetic scattering and doppler analysis of three-dimensional breaking wave crests at low-grazing angles," *Progress In Electromagnetics Research*, Vol. 119, 239–252, 2011.